Available online at www.sciencedirect.com
SCIENCE DIRECT®
Journal of Magnetic Resonance 174 (2005) 28–33
JMR Journal of Magnetic Resonance
www.elsevier.com/locate/jmr

Measurements and modeling of long range ^{3}He diffusion in the lung using a "slice-washout" method

Stanislao Fichele, Martyn N.J. Paley, Neil Woodhouse, Paul D. Griffiths, Edwin J.R. van Beek, Jim M. Wild*

Academic Unit of Radiology, The University of Sheffield, Royal Hallamshire Hospital, Glossop Road, Sheffield S10 2JF, UK

Received 4 November 2004; revised 16 December 2004
Available online 1 February 2005

Abstract

In healthy lung tissue, pulsed-gradient-spin-echo (PGSE) methods reveal apparent diffusion coefficients (ADC) of the order 0.20 $cm^2\ s^{-1}$; for diffusion times of ≈2 ms. For these short diffusion times the ADC is only sensitive to structures approximately $(2Dt)^{1/2} \approx 0.6$ mm in size. Recent work, using magnetic tagging of the longitudinal magnetization has revealed much smaller ADC values for longer length scales. In this work, the in vivo ADC from within the air-spaces, was measured using a new technique. The signal from a series of images was analyzed from a slice that was repeatedly imaged. Diffusion tends to "top-up" the non-renewable polarization within the slice, which leads to a non-exponential decay in image signal. Image data were compared to 1D finite-difference simulations of diffusion to calculate a long range ADC value. The results yield values of the order 0.034 $cm^2\ s^{-1}$, which are nearly an order of magnitude smaller than those reported by PGSE measurements at shorter diffusion times.

Keywords: Helium; Hyper-polarized; Diffusion; ADC; PGSE

1. Introduction

^{3}He gas diffusion measurements have the potential to enhance our understanding of lung physiology and monitor the progression of diseases that destroy lung tissue [1,2]. Helium is a fast-diffusing element, which encounters the alveolar walls many times during a typical MR repetition time. Consequently, diffusion is restricted and the measured apparent diffusion coefficient (ADC) is considerably smaller than the self-diffusion coefficient in room air, since it is sensitive to the alveolar dimensions and structure [3–5].

In hyper-polarized gas imaging, the ADC is typically measured using pulsed-gradient-spin-echo (PGSE) techniques, which employ relatively short diffusion times of 2–5 ms. In healthy lung tissue the ADC values are in the range 0.1–0.25 $cm^2\ s^{-1}$ [3,4,6,7]. The consequence of the short diffusion time is the ADC is only influenced by structures that are of the order of $\sqrt{2Dt} \approx 0.6$ mm in length, which is approximately the size of two alveoli. Hence, the majority of previously reported measurements reveal little about diffusion on longer length scales such as between neighboring acinar sacs.

The acinar structure comprises hundreds of alveolar ducts [8], each branching dichotomously to further ducts. The acinar sac is approximately 7 mm in diameter, and usually there is only one "entrance." Hence, in order for gas to diffuse from deep within one acinus to another it must undergo a "long" and tortuous path. In certain applications it would be useful to determine a typical value for the inter-acinar diffusion coefficient. For example, in the measurement of oxygen partial pressure (pO_2), the polarization is monitored over a "long" time-course of typically 10–20 s [9]. Diffusion will tend to mix regions of differing pO_2, however, the rate at

* Corresponding author. Fax: +44 114 272 4760.
E-mail address: j.m.wild@sheffield.ac.uk (J.M. Wild).

1090-7807/$ - see front matter © 2005 Elsevier Inc. All rights reserved.
doi:10.1016/j.jmr.2004.12.011

which this might occur could be greatly over estimated by the PGSE ADC measurement as discussed in [10].

So far, the only reported measurements in the lungs using longer diffusion times have been performed using spatially modulated magnetization (SPAMM) [11–13]. In this method diffusion acts to attenuate the amplitude of sinusoidal magnetization as a function of time. By monitoring the evolution of the amplitude, an ADC value can be determined. Owers-Bradley et al. [11] studied healthy volunteers, while Woods et al. [13] looked at diffusion in healthy and diseased canine models. In both cases the measurements revealed ADC values of the order 0.01 $cm^2 s^{-1}$, which are an order of magnitude smaller than that reported by PGSE methods, reported at short diffusion times. The low value demonstrates that the 'diffusive interconnectivity' between acini is much smaller than restricted diffusion within the alveolar ducts.

Another method for exploring diffusion on long length scales involves "burning out" magnetization within a slice and monitoring the evolution of the slice profile. This technique was used by Schmidt et al. [14] and Pfeffer and Lutz [15] to measure ^{129}Xe and ^{3}He diffusion in vitro at high gas pressures. In this work we used a similar method to measure the long range ADC in vivo with long diffusion times (8 s). The technique is conceptually similar to monitoring the decay of sinusoidal tags; the only difference is the method used to calculate the ADC. The same slice can be repeatedly imaged using a standard gradient echo sequence, so that the continual application of RF pulses gradually "burn out" the magnetization within the imaging slice. The polarization for hyper-polarized gas is non-renewable, so in the absence of diffusion the in-slice magnetization decays (almost) exponentially [16]. However, diffusion acts to continually smear out the "hard" slice profile, which in turn means the magnetization within the slice profile is "topped up" at the expense of the out-of-slice magnetization reserve. It is possible to model the changing profile of magnetization as a result of T_1 relaxation, diffusion and RF excitation using a simple finite-difference method in 1D; and thus calculate the effect on signal intensity for a time series of images. The simulation method, coupled with a simple least-squares fitting algorithm, can be used to calculate the ADC from in vivo data. We have used a similar numerical method previously to predict inter-slice diffusion as a source of signal loss in 2D imaging [17] and to examine the effects of diffusion on in vivo estimates of pO_2 that use 2D sequences [10].

2. Methods

2.1. Imaging

Volunteers and in vitro tests were performed at 1.5 T using a whole-body system (Philips Eclipse, Cleveland, OH). Gas was polarized to approximately 30% using a prototype commercial spin exchange system (GE Health). With local ethical approval a total of five healthy volunteers were scanned. In vitro measurements were also undertaken in hollow plastic cylinders (60 ml syringes), which were 11 cm in length and 2.5 cm in diameter.

To accurately deduce the ADC from the in vivo signal evolution it was necessary to calibrate the actual flip-angle in the lungs and the T_1 relaxation time. This necessitated a total of three image data sets to be acquired from each volunteer. These will be referred to as the "T_1-image," the "low-flip image," and the "high-flip image." The three images were all acquired using a fast-low-angle-shot (FLASH) sequence.

2.1.1. T_1-image

To calculate T_1 relaxation in a particular region of interest, we required FLASH parameters that caused negligible de-polarization and created signal evolutions that were insensitive to flip-angle variations and diffusion. These requirements were satisfied with an ultra-low flip-angle and a relatively thick slice. Parameters were: ≈0.5° flip-angle, 6 ms repetition time (TR), 2.5 ms time-to-echo (TE), 32.15 kHz bandwidth, $N_y = 20$ phase encode steps, 42 cm field of view, and a 60 mm slice thickness. In all, 10 images were acquired at 1.00 s intervals. The small number of phase encode steps and the ultra-low flip-angle meant that the effects of RF de-polarization were negligible when calculating T_1. An adequate signal-to-noise ratio in the images was achieved with 200 ml of ^{3}He gas polarized to 30%. The ^{3}He gas was diluted with 600 ml N_2 prior to delivery. Numerical simulations (which are not shown here) were used to confirm that diffusion over the 600 mm slice would have little effect on the normalized signal evolution, hence, allowing the calibration of T_1.

MR imaging was performed using a flexible transmit-receive coil that was in close contact with the subject. There were large variations in coil loading between subjects and it was necessary to determine the exact flip-angle in the lungs, or provide image data that was less sensitive to flip-angle when fitting for diffusion. Using two sequences; one employing a "low" flip-angle and the other a "high" flip-angle it was possible to simultaneously calculate the flip-angle and the long range diffusion coefficient, D. The dose comprised 300 ml of ^{3}He and 500 ml of N_2, which yielded an adequate signal-to-noise ratio for a region-of-interest analysis.

2.1.2. Low-flip image

A spoiled FLASH sequence with crusher gradients was used. Parameters were: 5° (nominal) flip-angle, 11 ms repetition time (TR), 8.0 ms time-to-echo (TE), 32.15 kHz bandwidth, 42 cm field of view, $N_y = 64$ phase encode steps, and a 13.1 mm slice thickness. In all 10 images were acquired at 0.8 s intervals.

2.1.3. High-flip image

The same parameters as the "low-flip image" were used, except the flip-angle was exactly twice as large, at 10° (nominal).

The diffusion coefficient in vitro was measured using two acquisitions, each consisting of 10 images, all acquired at position $z = 0$. The parameters for each image were: flip-angle 5.1°; number of k-space lines $N_y = 100$; TR = 11 ms; delay between images TD = 150 ms. The first set of images were acquired with no slice selection, while the second set of images were acquired with a 13.1 mm slice.

2.2. Simulating "slice washout"

In an ideal experiment, where the RF excitation pulse creates a perfect, "hard" slice selection, the evolution of the magnetization could be calculated analytically from the diffusion equation [14,15,17]. However, since slice profiles are usually non-uniform (e.g., sinc-gaussian), the pursuit of analytical methods could be problematic. As an alternative, finite-difference methods [18–22] offer a simple, but effective method for calculating the profile evolution in one-dimension.

We simulated the evolution of M_z along the slice direction (z-axis), and its effect of on the MR signal for a gradient spoiled, centric-reordered FLASH sequence. The sequence consisted of N images acquired from the same location. Each image block comprised N_y phase steps, each of duration, TR. There was also a short delay of TD between successive image blocks. The magnetization was represented by N_z sequential elements, spaced evenly by an amount Δz. The entire simulation process can be broken into the following steps:

Step 1: each magnetization element was initialized to unity, since prior to imaging, the longitudinal magnetization was assumed to be uniform.

Step 2: at the start of each image block, the normalized pixel signal intensity was calculated. Given that the signal-to-noise ratio in a centric-reordered FLASH image is proportional to the central line in k-space [16], the SNR could be obtained by the following summation

$$\mathrm{SNR} = k\exp(-bD')\sum_{i=0}^{N_z} M_i \sin\alpha_i, \tag{1}$$

where M_i is the magnetization of the ith element; α_i is the flip-angle at ith position; D' is the ADC as measured by PGSE; and b is the "b-value" that characterizes the attenuation associated with the readout, phase, and slice-select gradients. The term, $\exp(-bD')$, could be eliminated by normalizing the signal against the SNR from the first image. Hence the normalized signal, S, becomes

$$S = \frac{\sum_{i=0}^{N_Z} M_i \sin\alpha_i}{\sum_{i=0}^{N_Z} \sin\alpha_i} \tag{2}$$

which is independent of the effect that diffusion has on the transverse magnetization.

Step 3: for each line of k-space, the application of the RF pulse was simulated by applying the multiplication factor $\cos(\alpha_i)$ to each element M_i. The effect of diffusion during the RF pulse was assumed to be adequately described by the term $\exp(-bD')$ given above, and could hence be ignored.

Step 4: the time difference between successive RF excitations was TR, during which the longitudinal magnetization decays through T_1 relaxation and is dispersed by diffusion. Here, a 1D finite-difference method was used to simulate diffusion over the duration TR. Thereafter, the effect of T_1 relaxation was incorporated by applying the factor $\exp(-\mathrm{TR}/T_1)$ to each element; this implied a fixed T_1 over the duration of the breath-hold. Diffusion was simulated in 1D with the following first-order equations [19]:

$$M_i' = M_i^n + D\frac{\Delta t}{\Delta z^2}(M_{i-1}^n - M_i^n), \tag{3}$$

$$M_i^{n+1} = M_i' + D\frac{\Delta t}{\Delta z^2}(M_{i+1}^n - M_i^n), \tag{4}$$

where the superscript n denotes the nth time step, i.e., $t = n\Delta t$; M_i' is an intermediate quantity; and D is the apparent, long-range diffusion coefficient. For our purposes sufficient accuracy was obtained with parameters $\Delta z = 0.5$ mm, $\Delta t = 1$ ms, and $N_z = 220$. For simplicity, Eq. (3) was not applied to the first (leftmost) element, and Eq. (4) was not applied to the last (rightmost) element. This was equivalent to placing impenetrable barriers at $i = 0$ and $i = N_z + 1$, which can lead to edge effect problems, however, in this application the associated effect on the magnetization profile was found to be negligible and could be ignored.

Step 5: this step was identical to step 3, except the duration was TD, which is the short delay between the end of the last image and start of the next image.

Steps 3 and 4 were repeated N_y times for each line of k-space. Steps 2 and 5 were repeated N times, once for each image block. The slice flip-angle distribution, α_i was calculated by Fourier transform of the RF pulse, which was considered a valid approximation for the small flip-angles being used [23]. The slice thickness was defined as the full width at half the maximum slice "height" (FWHM). This approach fully encompassed the change in slice profile that is caused by polarization depletion, which has been described previously [16].

Gradient crushers were used to null any transverse magnetization before the commencement of the next RF excitation; therefore, no transient or steady state effects needed to be taken into account. This was reasonable since gradient crushers were employed. T_2^*

relaxation could also be ignored in the analysis since its effect was absorbed into the constant k, which factors out of the normalized signal intensity equation, Eq. (2).

2.3. Analysis of data

Calculation of the long range in vivo diffusion coefficient, D, was achieved by fitting the image data using a least-squares Nelder–Mead simplex search [24]. First, regions of interest were selected in the lung, and the mean signal intensity was calculated from the low-flip and high-flip images, I_{Ln} and I_{Hn}, respectively, where n is the nth image. These were normalized such that I_{L1} was unity. The diffusion simulation was performed for parameters that were chosen by the Nelder–Mead simplex algorithm, which produced two normalized signals, S_L and S_H, corresponding to the low-flip image parameters and the high-flip image parameters, respectively. The fitting error was calculated as

$$\text{error} = \sum_{n=1}^{N} (S_{Ln} - I_{Ln})^2 + (S_{Hn} - I_{Hn})^2. \quad (5)$$

The simulations made the assumption that the ratio of flip-angles in the images was exactly 2. Stability tests on the output of our RF amplifier at very low flip-angles have previously shown that this assumption is valid [10]. By fitting two image data sets simultaneously, the accuracy of the fit was greatly improved.

3. Results

The results of the in vitro test are shown in Fig. 1. Experimental data versus theory is plotted, along with the simulated profile of the magnetization at the commencement of each imaging block. The experimental data for the thick (300 mm) slice was used to accurately determine the flip-angle of the sequence, since diffusion had little (or no) effect on the signal evolution. Using this flip-angle, and ignoring T_1 relaxation, the data for the thin (13.1 mm) slice were fitted using the diffusion simulation by a least-squares Nelder–Mead search. The numerical results yielded a diffusion coefficient of 1.95 $cm^2\ s^{-1}$, which was in good agreement with published and theoretical values [25]. In addition, the simulation data were an excellent fit to the experimental data, and were taken as a validation of the method.

The in vivo results are summarized in Table 1. The average ADC for the healthy volunteers was found to be 0.034 $cm^2\ s^{-1}$. Data from one volunteer are shown in Fig. 2. Here the T_1 relaxation time was measured to be 25 s using data from the T_1-image series. The low-flip and high-flip image data were fitted against simulations, where the flip-angle and ADC were determined using a Nelder–Mead least-squares search. Again, the simulation results were in good agreement with all the experimental data. To demonstrate that the small ADC (0.033 $cm^2\ s^{-1}$) does cause a significant perturbation to the signal inten-

Table 1
The average "long range" ADC value found for each volunteer

Gender	Age	Average ADC ($cm^2\ s^{-1}$)
F	27	0.033 ± 0.008
M	33	0.035 ± 0.008
M	35	0.036 ± 0.008
M	28	0.033 ± 0.008
F	52	0.033 ± 0.008

M=Male, F=Female.

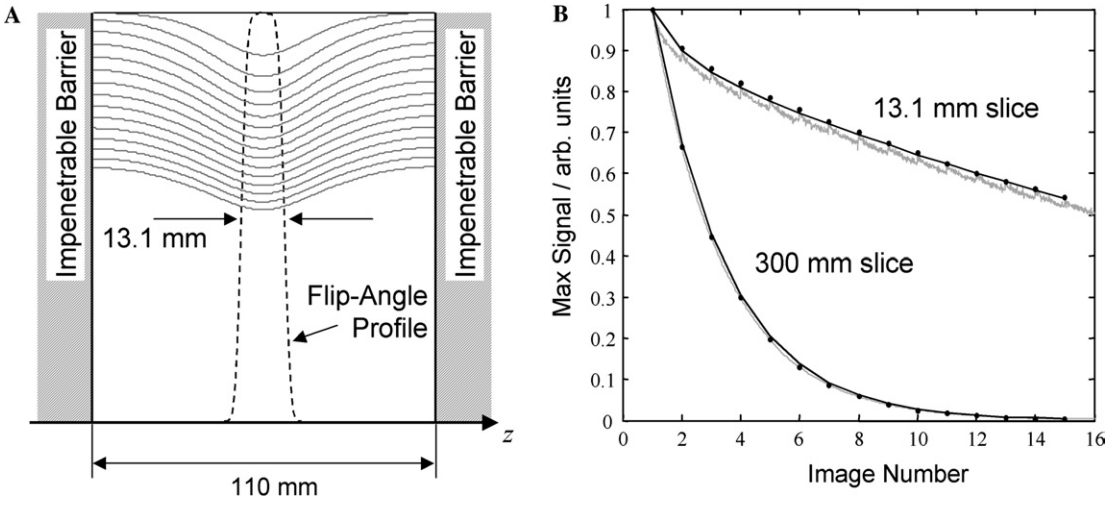

Fig. 1. In vitro results against theory for a hollow cylindrical sample. (A) The magnetization profile at the start of each image, as calculated by the finite-difference method ($N_z = 220$, and $\Delta z = 0.5$ mm). The flip-angle profile, α, is also shown as a dotted line. MRI sequence: $N_y = 100$, TR = 11 ms, flip = 5.1°, images acquired at 1.25 s intervals. (B) The signal intensity results from in vitro displayed against theory, with $D_0 = 1.95\ cm^2\ s^{-1}$. The gray line is the amplitude of each FID. The data are in excellent agreement with the simulation results.

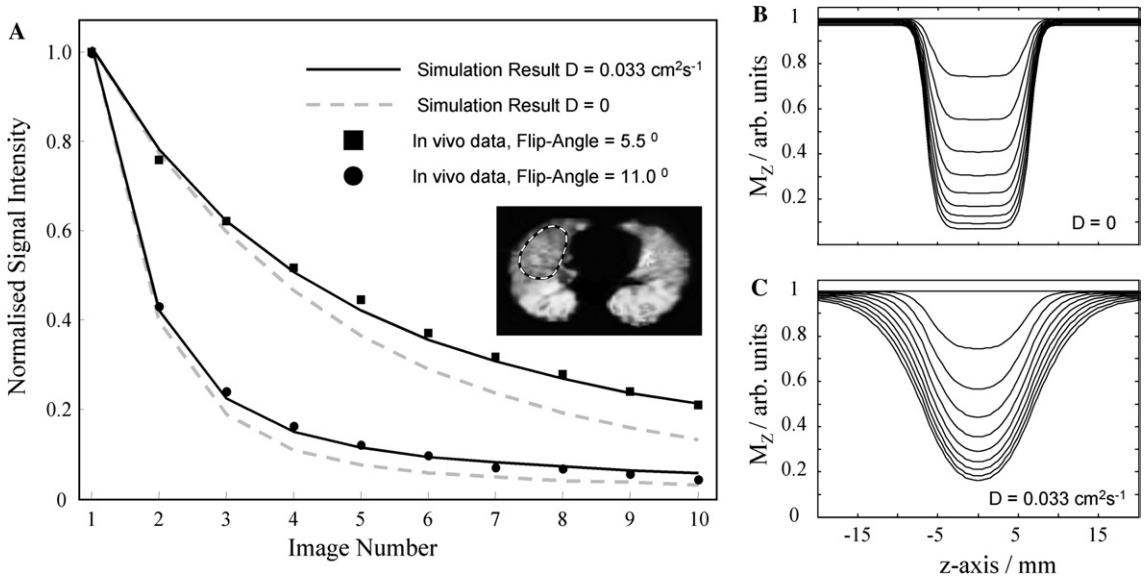

Fig. 2. (A) In vivo data, each image was acquired at 1.25 s intervals. The data were analyzed using a T_1 value of 25 s. Despite the ADC being small, its effect on the data is clearly evident when compared to the gray-dashed line, plotted for $D = 0$. (B and C) The simulated profiles of the magnetization, plotted at the commencement of each image block, for $D = 0$ and $D = 0.033\ \mathrm{cm^2\ s^{-1}}$, respectively. The flip-angle was 5.5°.

sity, simulations for $D = 0$ are also plotted for comparison.

4. Discussion and conclusions

We have demonstrated that the slice-washout method can be used to determine the long range diffusion coefficient in vivo. Finite-difference simulations were used to model the evolution of the slice profile, which allowed great flexibility in the choice of RF pulses used to excite the slices. On average, the long-range ADC in vivo was found to be $0.034\ \mathrm{cm^2\ s^{-1}}$, which was almost an order of magnitude smaller than that measured by PGSE methods, which have typically used short diffusion times. The low ADC value suggests that gas diffuses slowly between neighboring acini, which is reasonable when we consider the structure of the acinar sac. As mentioned above the acini comprise a labyrinth of alveolar ducts which are organized in a branching pattern. An ideal acinus has only one "entrance/exit," hence, to travel a distance of a few centimeters the ^{3}He gas must diffuse via a highly tortuous path. In effect the acinar sac acts like an *Oubliette*—"a prison which it is extremely difficult to escape from," which, accounts for the small, long-range, diffusion coefficient.

Woods et al. and Owers-Bradley et al. also found low ADC values, which were of the order $0.01\ \mathrm{cm^2\ s^{-1}}$ in healthy humans and animals. Their values were lower than the values found here, which is likely due to experimental differences. For example, in the reported tagging experiments, wavelengths of the order of a few centimeters were used to measure diffusion. Here, diffusion was measured using a slice thickness of 13 mm, which is a much shorter length scale.

A drawback of this methodology is it requires a high signal-to-noise ratio in order to make an accurate measurement. It should be possible to create a 2D map of the ADC on a pixel-by-pixel basis, however, a larger amount of polarized gas would be required. In addition, only one slice through the lungs can be assessed, whereas with a standard PGSE sequence the entire lung volume can be covered. A further problem with the method presented is the use of three images to calculate the ADC. However, it later became evident that it was not necessary to calibrate the T_1 relaxation rate in the lungs, as the flip-angle and T_1 are not independent parameters in the fitting procedure. Hence, T_1 need not be measured and could instead be assumed infinite. Thereafter, fitting the data yields exactly the same ADC value but reveals an adjusted value for flip-angle which "absorbs" the effect of T_1 relaxation. Since we are not interested in measuring the actual flip-angle or T_1 this is perfectly acceptable, hence we do not need to perform the first image set ("T_1-image").

It was also unnecessary to acquire the "high-flip image," since it was possible to find the ADC adequately from fitting just the "low-flip image." However, the results were less prone to error if "low-flip image" and "high-flip image" were fitted together.

There is a marked difference between the method presented here and the methods found in [14,15]. In Schmidt's and Pfeffer's methods the entire profile of the magnetization in the z-direction was monitored as a function of time. In this method only the time-course of a given pixel signal intensity was analyzed. This

potentially allows the ADC to be calculated on a pixel-by-pixel basis throughout the image slice.

In conclusion, slice-washout techniques are useful for measuring diffusion in vivo. We used finite-difference methods to simulate the process, bypassing the need for a complicated analytical analysis of the diffusion process.

Acknowledgments

We acknowledge the following companies: *GE Healthcare* for generous support of polarising equipment; *Spectra-Gases* for support with ^{3}He gas; and *Philips Medical Systems* for scanner support.

References

[1] H.E. Moller, X.J. Chen, B.T. Saam, K.D. Hagspiel, G.A. Johnson, T.A. Altes, E.E. De Lange, H.U. Kauczor, MRI of the lungs using hyperpolarized noble gases, Magn. Reson. Med. 47 (2002) 1029–1051.

[2] H.U. Kauczor, X.J. Chen, E.J.R. van Beek, W. Schreiber, Pulmonary ventilation imaged by MRI: at the doorstep of clinical application, Eur. Respir. J. 17 (2001) 1–16.

[3] B.T. Saam, D.A. Yablonskiy, V.D. Kodibagkar, J.C. Leawoods, D.S. Gierada, J.D. Cooper, S.S. Lefrak, M.S. Conradi, MR imaging of diffusion of ^{3}He gas in healthy and diseased lungs, Magn. Reson. Med. 44 (2000) 174–179.

[4] J.P. Mugler III, J.R. Brookemann, J. Knight-Scott, T. Maier, E.E. De Lange, P.L. Bogorad, Regional measurement of the ^{3}He diffusion coefficient in the human lung, in: 6th Meeting of ISMRM, 1998, Sydney.

[5] D.A. Yablonskiy, A.L. Sukstanskii, J.C. Leawoods, D.S. Gierada, G.L. Bretthorst, S.S. Lefrak, J.D. Cooper, M.S. Conradi, Quantitative in vivo assessment of lung microstructure at the alveolar level with hyperpolarized ^{3}He diffusion MRI, Proc. Natl. Acad. Sci. USA 99 (2002) 3111–3116.

[6] M. Salerno, E.E.D. Lange, T.A. Altes, J.D. Truwit, J.R. Brookemann, J.P. Mugler III, Emphysema: hyperpolarized helium 3 diffusion MR imaging of the lungs compared with spirometric indexes-initial experience, Radiology 222 (2002) 252–260.

[7] C.P. Bidinosti, J. Choukeife, P.J. Nacher, G. Tastevin, In vivo NMR of hyperpolarized ^{3}He in the human lung at very low magnetic fields, J. Magn. Reson. 162 (2003) 122–132.

[8] A.B. Lumb, Applied Respiratory Physiology, Butterworth-Heinemann, Oxford, 2000.

[9] A.J. Deninger, B. Eberle, M. Ebert, T. Großmann, W. Heil, H.-U. Kauczor, L. Lauer, K. Markstaller, E. Otten, J. Schmiedeskamp, W. Schreiber, R. Surkau, M. Thelen, N. Weiler, Quantification of regional intrapulmonary oxygen partial pressure evolution during apnea by ^{3}He MRI, J. Magn. Reson. 141 (1999) 207–216.

[10] J.M. Wild, S. Fichele, S. Woodhouse, M.N.J. Paley, L. Kasuboski, E.J.R. van Beek, 3D volume localized pO_2 measurement in the human lung with ^{3}He MRI. Magn. Reson. Med. (2005), in press.

[11] J.R. Owers-Bradley, S. Fichele, A. Bennattayalah, C.J. McGloin, R.W. Bowtell, P.S. Morgan, A.R. Moody, MR tagging of human lungs using hyperpolarized ^{3}He gas, J. Magn. Reson. Imag. 17 (2003) 142–146.

[12] J.R. Owers-Bradley, A. Bennattayalah, S. Fichele, C.J. McGloin, R.W. Bowtell, P.S. Morgan, A.R. Moody, Diffusion and tagging of hyperpolarised ^{3}He in the lungs, in: International Society for Magnetic Resonance in Medicine, 2002, Honolulu, p. 2016.

[13] J.C. Woods, D.A. Yablonskiy, K. Chino, T.S.K. Tanoli, J.D. Cooper, M.S. Conradi, Magnetization tagging decay to measure long-range ^{3}He diffusion in healthy and emphysematous canine lungs, Magn. Reson. Med. 51 (2004) 1002–1008.

[14] D.M. Schmidt, J.S. George, S.I. Penttila, A. Caprihan, E. Fukushima, Diffusion imaging with hyperpolarized ^{3}He gas, J. Magn. Res. (1997) 129.

[15] M. Pfeffer, O. Lutz, Observation of diffusion in xenon gas by NMR, J. Magn. Res. 113 (1995) 108–113.

[16] J.M. Wild, M.N.J. Paley, M. Viallon, W.G. Schreiber, E.J.R. van Beek, P.D. Griffiths, *k*-space filtering in 2-D gradient-echo breath-hold hyperpolarized ^{3}He MRI: spatial resolution and signal-to-noise ratio considerations, Magn. Reson. Med. 47 (2002) 687–695.

[17] J.M. Wild, N. Woodhouse, M.N. Paley, S. Fichele, Z. Said, L. Kasuboski, E.J. van Beek, Comparison between 2D and 3D gradient-echo sequences for MRI of human lung ventilation with hyperpolarized ^{3}He, Magn. Reson. Med. 52 (2004) 673–678.

[18] S. Fichele, M.N.J. Paley, N. Woodhouse, P.D. Griffiths, E.J.R. van Beek, J.M. Wild, Investigating ^{3}He diffusion NMR in the lungs using finite difference simulations and in-vivo PGSE experiments, J. Magn. Res. 167 (2003) 1–11.

[19] J. Crank, The Mathematics of Diffusion, second ed., Oxford University Press, London, 1975.

[20] H. Hagslatt, B. Jonsson, M.O.S. Nyden, Predictions of pulsed field gradient NMR echo-decays for molecules diffusing in various restrictive geometries. Simulations of diffusion propagators based on a finite element method, J. Magn. Res. 161 (2003) 138–147.

[21] G.P. Zientara, J.H. Freed, Spin-echoes for diffusion in bounded, heterogeneous media: a numerical study, J. Chem. Phys. 72 (1980) 1285.

[22] C.L. Chin, F.W. Wehrli, S.N. Hwang, M. Takahashi, D.B. Hackney, Biexponential diffusion attenuation in the rat spinal cord: computer simulations based on anatomic images of axonal architecture, Magn. Reson. Med. 47 (2002) 455–460.

[23] P. Callaghan, Principles of Nuclear Magnetic Resonance Microscopy, Oxford University Press, Oxford, 1991.

[24] J.A. Nelder, R. Mead, A simplex method for function minimization, Comput. J. 7 (1965) 308–313.

[25] J.C. Liner, S. Weissman, Determination of the temperature dependence of gaseous diffusion coefficients using gas chromatographic apparatus, J. Chem. Phys. 56 (1972) 2288–2290.